Proceedings of the 2011 IEEE
International Conference on Robotics and Biomimetics
December 7-11, 2011, Phuket, Thailand

Robotic Table Tennis based on Physical Models of Aerodynamics and Rebounds

Akira Nakashima, Yuki Ogawa, Chunfang Liu and Yoshikazu Hayakawa

Abstract— **In this paper, we develop a robotic table tennis system based on explicit physical models of the ball motion with our developed real-time measuring method of the flying rotated ball. In order for a robot with a racket to hit the ball to a target point, a determination method of the racket motion is proposed. The motion determination method is performed by two sub inverse problems of the physical models. The first inverse problem is to solve the aerodynamics with respect to the velocity just after the time when the ball is hit. With the solved velocity, the second inverse problem is to solve the racket rebound model with respect to the orientation and velocity of the racket. In these problems, the elevation angle of the racket and the launch angle of the hit ball are the redundant parameters. The racket velocity is minimized with respect to these parameters in order not to break the speed limitation due to the robot performance. The effectiveness of the method is verified by some experiments.**

I. Introduction

Dynamic manipulation is dexterous task of humans by utilizing dynamics of manipulated targets [1]. In ball sports for examples in the dynamic manipulation, there are intermittent interactions between the ball and environments. The ball is manipulated by the interactions between the ball and players, which have to be performed by taking into account the dynamics of the ball. Especially in the case of table tennis, since the ball speed is fast and the distance between players is close, the fight time of the ball is very short. For example, it is about 520 [ms] in the case of the usual speed 5.0 [m/s] [2]. It is therefore essential to rapidly recognize the ball in the opponent's court and predict the ball trajectory in order to plan the racket motion at the hitting time. Since these issues are very attractive and challenging, many researchers study and develop robots playing table tennis [3].

The robotic table tennis system consists of 1) the ball recognition, 2) the ball motion prediction and 3) the racket motion determination. 1) The ball recognition is the measurement of the position, translational/rotational velocities of a flying ping-pong ball, which is usually performed by vision cameras. 2) The detected information is necessary for the ball motion prediction, which is utilized for gaining the ball's position and velocities at the time when a robot hits the ball. With the gained states, 3) the racket motion determination is performed which solves the position, orientation and velocity of the racket attached to the robot in order to hit the ball to a target point on the opponent's table area. The prediction and motion determination have been dealt with by two methodologies; the one is based on input-output black-box or grey-box models and the other is based on explicit physical models of the aerodynamics and rebound of the ball.

Authors are with Mechanical Science and Engineering, Graduate School of Engineering, Nagoya University, Furo-cho, Chikusa-ku, Nagoya, Japan akira@haya.nuem.nagoya-u.ac.jp, and Y. Hayakawa is also with RIKEN-TRI Collaboration Center, RIKEN, 2271-103, Anagahora, Shimoshidami, Moriyama-ku, Nagoya, Japan hayakawa@nuem.nagoya-u.ac.jp.

Miyazaki et al. [4] developed a robotic table tennis system in which the ball prediction is performed by the input-output maps using a k-dimensional tree model. In their next study [5], the ball prediction and motion determination are performed by three maps of the locally weighted regression, which express the ball trajectories before and after the rebound on the racket and the velocity variation of the ball due to the rebound. Their approaches can be interpreted as learning methods using black-box or grey-box models with experimental data. However, the rotational velocity is not considered in [5] although it effects on the ball trajectory in the cases of the flight and rebound.

A pioneering robotic table tennis system was developed by H. Hashimoto et al. [6]. The ball prediction is performed by physical models of the flying motion and rebound on the table. R. L. Anderson [7] developed a robotic table tennis system where the prediction and motion determination are performed as sequential decisions by physical models of the ball motion and rebound. Z. Zhang et al. [8], [9] developed a visual measurement system and a prediction method of the ball trajectory using the ball motion with the air resistance and the rebound. However, in these studies, the rotational velocity is not considered in the physical models of the aerodynamics and the rebound.

There are two reasons that the rotational velocity is not considered. As for the first reason, there were no available measuring methods. However recently, a high speed camera (1000fps) has been developed [10] and a real-time measuring of the rotational velocity [11] has been proposed. Using same two high speed cameras, we have developed real-time measuring methods [12], [13], where both the translational and rotational velocities can be measured. As for the second reason, there were no models of the ball motions with the rotational velocity which are available for the prediction and racket determination. We have modeled the aerodynamics with the lift and drag effects considered [14] and the rebound phenomena of the rotated ball on the rigid table and the elastic racket [15]. In this paper, we develop a robotic table tennis system based on these physical models of the ball motion with the our developed real-time measuring method of the flying rotated ball. In order for a robot with a racket to hit the ball to a target point, a determination method of the racket motion is proposed. The motion determination

978-1-4577-2138-0/11/$26.00 © 2011 IEEE

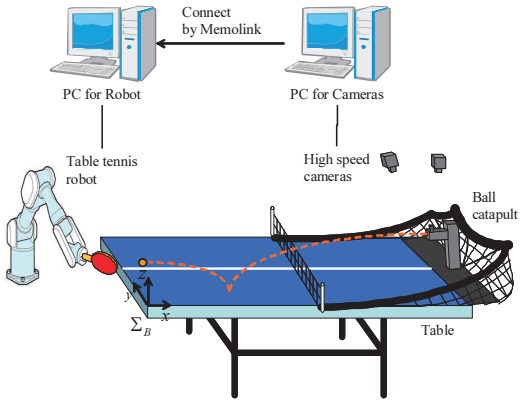

Fig. 1. A robotic table tennis system.

method is performed by two sub inverse problems of the physical models. The first inverse problem is to solve the aerodynamics with respect to the velocity just after the time when the ball is hit. With the solved velocity, the second inverse problem is to solve the racket rebound model with respect to the orientation and velocity of the racket. In these problems, the elevation angle of the racket and the launch angle of the hit ball are the redundant parameters. The racket velocity is minimized with respect to these parameters in order not to break the speed limitation due to the robot performance.

In Section 2, the configuration of the system is shown. The physical models of the aerodynamics and rebound are briefly shown in Section 3 for preliminary. In Section 4, the ball prediction is explained which is compared with the one without the effects of the rotational velocity. The inverse problems are solved in Section 5. In Section 6, experimental results are shown to verify the effectiveness of the proposed method. Conclusions and feature work are described in Section 7.

II. System Configuration

A. Experimental System

Figure 1 illustrates our robotic table tennis system. The table is an international standard one with the size of 1525(W)×760(H)×2740(D) [mm]. Σ_B is the reference frame at the corner of the table. The mass and radius of a ping-pong ball are $m = 2.7 \times 10^{-3}$[kg] and $r = 2.0 \times 10^{-2}$[m]. The ball is shot out from the automatic ball catapult of ROBO-PONG 2040 (SAN-EI Co.) which is set at the end of the opponent's court. The flying ball is measured by the two high-speed cameras with 900 [fps] (Hamamatsu Photonics K.K.). The array size is 252×252 and the pixel sizes per meter are $\alpha_u, \alpha_v = 2.0 \times 10^{-5}$ [pixel/m]. The focal length of the lens is $f = 3.5 \times 10^{-2}$ [m]. The sampled data are quantized as 2D image coordinates with the monochrome brightness of 8bit (0–255). The table tennis robot is a 7 degrees of freedom manipulator of PA10-7C (Mitsubishi Heavy Industries, Ltd.). The sampling time is 2 [ms] and the speed limitation of the tip is 1.0 [m/s]. A racket is attached to the tip and its board and rubber are Fukuhara-Ai Special (Butterfly, Ltd.) and Bryce Speed FX (Butterfly, Ltd.). The distance from the center to the edge of the racket is about 80 [mm].

The PC for controlling the robot is Dell Precision T5500 (CPU: Intel(R)Xeon E5503 2.66GHz, Memory: 2GB RAM) and the PC for measuring the ball is Dell Precision T5300 (CPU: Intel(R)Xeon E5430 2.66GHz, Memory: 2GB RAM). The OS of the PCs are Windows XP Professional sp2 and the program language is C++. The measured ball information is transmitted to the PC for the control by the memolink (Interface, Ltd.). The ball prediction and motion determination are executed in the PC for the control.

Figure 2 (a) is the ball with the marked feature areas which are used for calculating the rotational velocity. Examples of the measured images of the flying ball are illustrated in Fig. 2 (b), where the ball is flying from the right to the left. The upper and lower images are the ones of the left and right cameras and n is the number of the frame. The rotational velocity is estimated by minimizing the intensity residuals between the two successive frames (e.g., the pairs of $n = 1, 2$, $n = 2, 3$) [12], [13]. The errors of the components of the translational velocity are about 0.1 [m/s] in the case of the measurement of the magnitudes of 2.0–7.0 [m/s] [12]. The error of the magnitude of the rotational velocity is about 400 [rpm] in the case of the measurment of the magnitudes of 1500–3000 [rpm]. The error of The angles between the true and estimated values are the about 30 [deg]. The averaged calculation time is 15–30 [ms] which is enough short compared with the rally time of 520 [ms].

B. Scheme of Hitting back a Flying Ball

Figure 3 shows the scheme of hitting a flying ball. The items (1)–(3) are explained in the followings:

(1) **[Ball Measurement]** The position and translational/rotational velocities of the ball are measured around the catapult. The measured values are given to the PC of the control for (2) the ball prediction.

(2) **[Ball Prediction]** With the measured ball information, the ball trajectory to the hitting point is calculated by the physical models of the aerodynamics and the rebound on the table. The obtained position and translational/rotational velocities at the hitting point are given to (3) the motion determination of the racket.

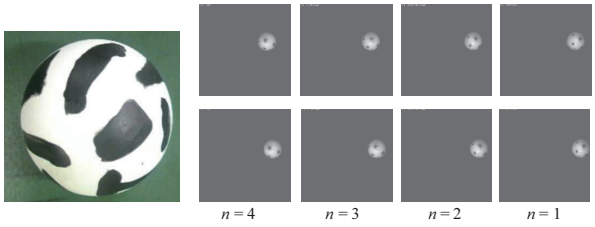

(a) Feature areas (b) Examples of the measured images

Fig. 2. Examples of the measured images of the high speed cameras.

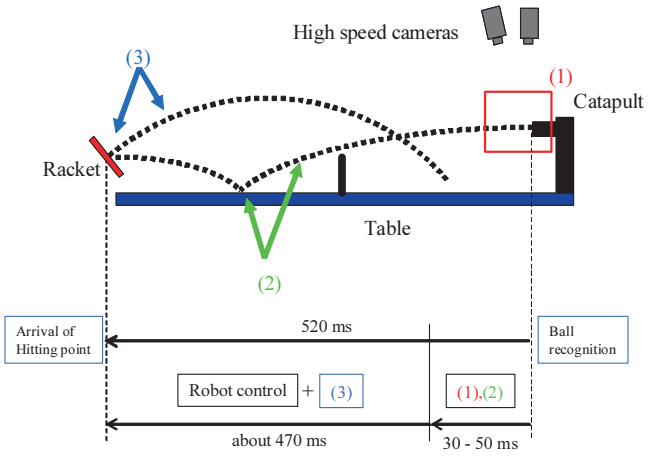

Fig. 3. Scheme of hitting back a flying ball.

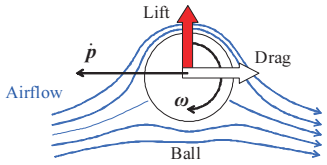

Fig. 4. The drag and lift forces of the rotated flying ball.

(3) **[Motion Determination]** With the predicted ball information, the racket motion is determined by solving the aerodynamics and the rebound of the racket as inverse problems.

The passage of time from the ball recognition to the arrival of the hitting is illustrated in the lower of Fig. 3. The amount of time for the items (1), (2) is about 30–50 [ms] because the processing time of (2) is 15–20 [ms] as in Section 4. Therefore, there is about 470 [ms] for (3) the motion determination and the robot control.

III. Physical Models of Table Tennis Ball

The physical models of the aerodynamics and the rebound of the table and racket are introduced here. The details of them are described in [14], [15].

A. Aerodynamics of Flying Ball

Define $\boldsymbol{p}_b \in \mathbb{R}^3$ and $\boldsymbol{\omega}_b \in \mathbb{R}^3$ as the position and rotational velocity of the ball. With the assumption that $\boldsymbol{\omega}_b$ is invariant, the equation of motion of the flying ball is given by

$$m\ddot{\boldsymbol{p}}_b = m\boldsymbol{g} - \frac{1}{2}C_D\pi\rho r^2\|\dot{\boldsymbol{p}}_b\|\dot{\boldsymbol{p}}_b + \frac{4}{3}C_M\pi\rho r^3\boldsymbol{\omega}_b \times \dot{\boldsymbol{p}}_b, \quad (1)$$

where $\boldsymbol{g} = [0, 0, -9.8]^{\mathrm{T}}$ [m/s^2] is the acceleration of gravity, $\rho = 1.184$ [kg/m^3] (25°C) is the air density, and C_D and C_M are the drag and lift coefficients. The second and third terms in the right hand of (1) are the lift and drag forces as illustrated in Fig. 4. The lift force is called as the Magnus effect, which can be large in the case of the large spin $\|\boldsymbol{\omega}_b\| = 3000$ [rpm] and the small mass $m = 2.7$ [g]. The C_D and C_M are identified as 0.54 and 0.069 in [14]. As an example of the case of a top spin ball, $\dot{\boldsymbol{p}}_b = [-5.0, 0, 0]^{\mathrm{T}}$ [m/s] and $\boldsymbol{\omega}_b = [0, -3000, 0]^{\mathrm{T}}$ [rpm], the drag and lift forces divided by the mass are calculated to 3.7 and 1.6. Since the lift force is about half of the drag one, ignoring the lift force can cause large errors in the prediction of the ball trajectory.

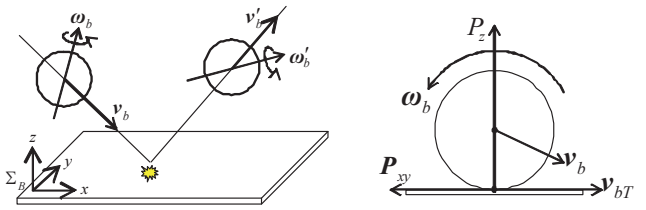

(a) Rebound on Table (b) Impulse in the tangent direction

Fig. 5. The rebound of the ball on the table.

B. Rebound Model of Table [15]

The rebound situation of the ball on the table is illustrated in Fig. 5 (a). Define $(\boldsymbol{v}_b, \boldsymbol{\omega}_b)$ as the translational and rotational velocities just before the rebound and $(\boldsymbol{v}'_b, \boldsymbol{\omega}'_b)$ as the those just after the rebound. The variables are expressed in the base frame Σ_B. The rebound models of the table and racket are expressed by

$$\begin{aligned}\boldsymbol{v}'_b &= \boldsymbol{A}_v\boldsymbol{v}_b + \boldsymbol{B}_v\boldsymbol{\omega}_b \\ \boldsymbol{\omega}'_b &= \boldsymbol{A}_\omega\boldsymbol{v}_b + \boldsymbol{B}_\omega\boldsymbol{\omega}_b.\end{aligned} \quad (2)$$

These are the algebraic equations where the $(\boldsymbol{v}'_b, \boldsymbol{\omega}'_b)$ is the input and $(\boldsymbol{v}_b, \boldsymbol{\omega}_b)$ is the output.

The rebound phenomenon in the normal direction is expressed by $v'_{bz} = -e_n v'_{bz}$ with the restitution coefficient $e_n > 0$. The other equations of the other components of $\boldsymbol{v}_b$ and $\boldsymbol{\omega}_b$ are derived by the conservation of momentum. If the contact is sliding, the impulse in the tangent direction is given by $P_{xy} = \mu P_z$ as shown in Fig. 5 (b), where P_z is the impulse in the normal direction and μ is the coefficient of the dynamical friction. The direction of P_{xy} is the inverse of the tangent velocity $\boldsymbol{v}_{bT}$ because it is caused by the dynamical friction. Note that the impulse P_{xy} is smaller than μP_z if the contact is rolling, i.e., the tangent velocity after the rebound $\boldsymbol{v}'_{bT}$ equals to 0. By these relationships, the coefficient matrices $\boldsymbol{A}_v$–$\boldsymbol{B}_\omega \in \mathbb{R}^{3\times3}$ are given by

$$\boldsymbol{A}_v = \bar{\boldsymbol{A}}_v(a),\ \boldsymbol{B}_v = \bar{\boldsymbol{B}}_v(a),\ \boldsymbol{A}_\omega = \bar{\boldsymbol{A}}_\omega(a),\ \boldsymbol{B}_\omega = \bar{\boldsymbol{B}}_\omega(a) \quad (3)$$

where

$$\begin{aligned}\bar{\boldsymbol{A}}_v(a) &:= \begin{bmatrix}1-a & 0 & 0\\ 1 & 1-a & 0\\ 0 & 0 & -e_n\end{bmatrix}, \bar{\boldsymbol{B}}_v(a) := \begin{bmatrix}0 & ar & 0\\ -ar & 0 & 0\\ 0 & 0 & 0\end{bmatrix} \\ \bar{\boldsymbol{A}}_\omega(a) &:= \begin{bmatrix}0 & -\frac{3a}{2r} & 0\\ \frac{3a}{2r} & 0 & 0\\ 0 & 0 & 0\end{bmatrix}, \bar{\boldsymbol{B}}_\omega(a) := \begin{bmatrix}1-\frac{3a}{2} & 0 & 0\\ 0 & 1-\frac{3a}{2} & 0\\ 0 & 0 & 1\end{bmatrix}.\end{aligned} \quad (4)$$

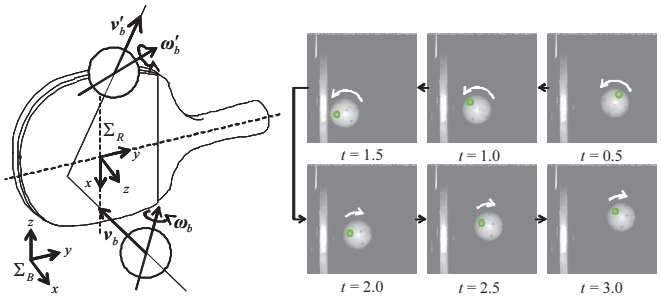

(a) Rebound on Racket (b) Inversion of the tangent velocity

Fig. 6. The rebound of the ball on the racket.

The parameter a is switched as

$$a = \mu(1+e_n)\frac{|v_{bz}|}{\|\boldsymbol{v}_{bT}\|}\ (\nu_s > 0), \quad \frac{2}{5}\ (\nu_s \le 0)$$
$$\nu_s = 1 - \frac{2}{5}\mu(1+e_n)\frac{|v_{bz}|}{\|\boldsymbol{v}_{bT}\|}.$$

$\nu_s > 0$ means the case of the sliding contact and $\nu_s \le 0$ means the case of the rolling contact. Note that the rebound model of the table is the piecewise linear equation with respect to a. The identified values are $\mu = 0.25$ and $e_n = 0.93$.

C. Rebound Model of Racket [15]

As illustrated in Fig. 6 (a), the variables of the velocities are the same in the previous subsection. Σ_R is the racket frame with the z-axis normal to the racket surface. In the case of the rebound on the racket, there is the effect of the elastic as in Fig. 6 (b), where the tangent and rotational velocities are inversed after the rebound. The equations of the rebound model to express this phenomenon are given by the following coefficient matrices:

$$\boldsymbol{A}_v = \boldsymbol{R}_R\bar{\boldsymbol{A}}_v(a)\boldsymbol{R}_R^{\mathrm{T}},\ \boldsymbol{B}_v = \boldsymbol{R}_R\bar{\boldsymbol{B}}_v(a)\boldsymbol{R}_R^{\mathrm{T}}$$
$$\boldsymbol{A}_\omega = \boldsymbol{R}_R\bar{\boldsymbol{A}}_\omega(a)\boldsymbol{R}_R^{\mathrm{T}},\ \boldsymbol{B}_\omega = \boldsymbol{R}_R\bar{\boldsymbol{B}}_\omega(a)\boldsymbol{R}_R^{\mathrm{T}} \qquad (5)$$

where the matrices with the bars are the same as those in (4) and

$$a = \frac{k_p}{m} \qquad (6)$$

is the fixed value differently from the case of the table. k_p is the coefficient which relates the tangent velocity to the tangent impulse. $\boldsymbol{R}_R(\beta,\alpha) \in \mathbb{R}^{3\times3}$ is the rotation matrix of Σ_R relative to Σ_B and (β,α) is the YX-Euler angle parameterization. Note that the rebound model of the racket is the nonlinear equation which consists of the sines and cosines of (β,α). The identified values are $e_n = 0.81$ and $k_p = 1.9\times10^{-3}$.

IV. Prediction of Spinning Ball

The prediction of the ball trajectory is performed by using the aerodynamic model of (1) and the rebound of the table of (2). The processing flow of the prediction is as follows:

1) Solve the differential equation of (1) with the initial state of the measured $\boldsymbol{p}_b$, $\boldsymbol{v}_b = \dot{\boldsymbol{p}}_b$ and $\boldsymbol{\omega}_b$ until the zero crossing appears in the z coordinate of $\boldsymbol{p}_b$. Memorize $\boldsymbol{p}_b$ and $(\boldsymbol{v}_b, \boldsymbol{\omega}_b)$ at the zero crossing as the velocities just before the rebound.
2) Obtain the velocities $(\boldsymbol{v}_b', \boldsymbol{\omega}_b')$ just after the rebound by substituting the memorized $(\boldsymbol{v}_b, \boldsymbol{\omega}_b)$ into (2).
3) Solve the differential equation of (1) with the initial state of the memorized $\boldsymbol{p}_b$ and the obtained $(\boldsymbol{v}_b', \boldsymbol{\omega}_b')$ until the z coordinate of $\boldsymbol{p}_b$ equals the hitting point, 0. Memorize $\boldsymbol{p}_b$ and $(\boldsymbol{v}_b, \boldsymbol{\omega}_b)$ at the hitting point.

In 1) and 3), the aerodynamics of (1) is solved by the 4th-order formula of Runge-Kutta method. The step size is fixed $1/150$ [s] for short processing time.

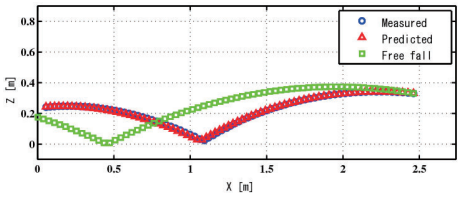

Fig. 7. The prediction of the ball trajectory of the top spin.

An example the top spin is shown for proving the effectiveness of the prediction. Figure 7 is the example of the top spin. The y coordinate is trivial and omitted for simplicity. The measured initial states are $\boldsymbol{p}_b = [2.46, 0.77, 0.33]^{\mathrm{T}}$ [m], $\boldsymbol{v}_b = [-5.43, 0.15, 0.92]^{\mathrm{T}}$ [m/s] and $\boldsymbol{\omega}_b = [-95, -2735, -121]^{\mathrm{T}}$ [rpm]. The blue circles, red triangles and green squares are the data of the measurement, prediction and free fall. In the data of the free fall, the simple rebound equation in the normal direction is only considered and the tangent velocity does not change at the rebound. The predicted trajectory is very close to the measured one while the one of the free fall is quite different. The error distance of the free fall at the hitting point is about 70 [mm] close to the edge of the racket. This implies that the racket may not be able to hit the ball.

V. Motion Determination of Racket

A. Overview of Determination

The motion determination is performed by solving the following two inverse problems:

(3-1) Suppose that the position $\boldsymbol{p}_b'$ just after the rebound on the racket and the desired point $\boldsymbol{p}_{bd} = [p_{bxd}, p_{byd}, 0]^{\mathrm{T}}$ on the table are given. Then, find

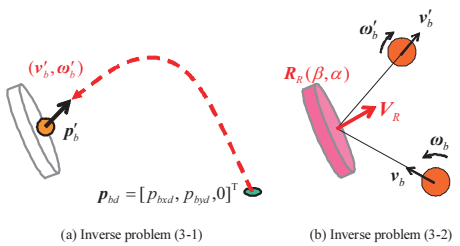

(a) Inverse problem (3-1) (b) Inverse problem (3-2)

Fig. 8. The inverse problems for the motion determination.

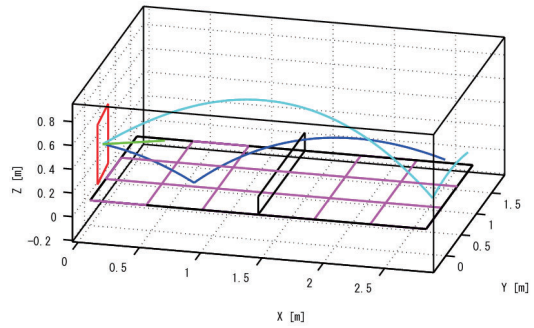

Fig. 9. An example of hitting back the shot ball.

the velocities $(\boldsymbol{v}_b', \boldsymbol{\omega}_b')$ just after the rebound on the racket with the equation of (4) (See Fig. 8 (a)).

(3-2) Suppose that the velocities $(\boldsymbol{v}_b, \boldsymbol{\omega}_b)$ and $(\boldsymbol{v}_b', \boldsymbol{\omega}_b')$ just before and after the rebound on the racket are given. Then, find the angles (β, α) and the velocity of the racket $\boldsymbol{V}_R$ with the equations of (2), (4), (5) and (6) (See Fig. 8 (b)).

It is difficult to solve these problems directly because of the followings:

(i) The calculation time has to be finished early to secure enough time for the control.
(ii) The racket velocity is limited as $\|\boldsymbol{V}_R\| \leq 1$ [m/s] due to the joint velocity limitation.
(iii) The aerodynamics of (4) is the nonlinear differential equation and there are the redundancy of the elevation angle of $\boldsymbol{v}_b'$ and the rotational velocity $\boldsymbol{\omega}_b'$.
(iv) The rebound of the racket of (2), (4), (5) and (6) consists of the complex simultaneous nonlinear equations.

In the latter subsections, the problems are solved as analytical solutions by some simplifications for overcoming the issues (i)–(iv).

B. Determination of Velocities after Rebound of Racket

The rotational velocity $\boldsymbol{\omega}_b'$ just after the rebound of the racket becomes quite small due to the limited racket velocity 1 [m/s]. Figure 9 shows an example of hitting back the shot ball with the initial conditions of $\boldsymbol{v}_b = [-5.29, -0.46, 1.93]^{\mathrm{T}}$ [m/s] and $\boldsymbol{\omega}_b = [248, -2838, 0]^{\mathrm{T}}$ [rpm]. The racket velocity is $\boldsymbol{V}_R = [0.98, 0.09, 0.12]^{\mathrm{T}}$ [m/s], which is almost the limitation. In this example, the translational and rotational velocities just after the rebound of the racket are $\boldsymbol{v}_b' = [4.74, 0.34, 3.12]^{\mathrm{T}}$ [m/s] and $\boldsymbol{\omega}_b' = [26, -234, -33]^{\mathrm{T}}$ [rpm]. Then, the lift force is about $1/10$ of the drag force.

Suppose that the desired point $\boldsymbol{p}_{bd}$ and the initial point $\boldsymbol{p}_{b0} = \boldsymbol{p}_b'$ are given. From the above discussion, the aerodynamics (1) can be approximated by

$$m\ddot{\boldsymbol{p}}_b = m\boldsymbol{g} - \frac{1}{2}C_D\pi\rho r^2\|\dot{\boldsymbol{p}}_b\|\dot{\boldsymbol{p}}_b. \tag{7}$$

Since the drag force in the z-axis is quite smaller the gravity force, it is ignored here. For simplicity, let use consider the coordinate transformation of p_{bs}, which is defined as the distance along $[\dot{p}_{bx}, \dot{p}_{by}, 0]^{\mathrm{T}}$, that is,

$$\begin{bmatrix}\dot{p}_{bx}\\ \dot{p}_{by}\end{bmatrix} = \dot{p}_{bs}\frac{\boldsymbol{p}_{bd0}}{\|\boldsymbol{p}_{bd0}\|},\ \boldsymbol{p}_{bd0} := \begin{bmatrix}p_{bxd} - p_{bx0}\\ p_{byd} - p_{by0}\end{bmatrix}. \tag{8}$$

Then, (7) is reduced to

$$\begin{aligned}\ddot{p}_{bs} &= -\frac{C_D\pi\rho r^2}{2m}\sqrt{\dot{p}_{bs}^2 + \dot{p}_{bz}^2}\dot{p}_{bs}\\ \ddot{p}_{bz} &= -g_z,\end{aligned} \tag{9}$$

where $g_z = 9.8$ [m/s^2]. Furthermore, the drag force is approximated to the one proportional to the initial velocity of the trajectory after the rebound:

$$\sqrt{\dot{p}_{bs}^2 + \dot{p}_{bz}^2}\dot{p}_{bs} \approx s\sqrt{v_{bs0}^2 + v_{bz0}^2}v_{bs0}, \tag{10}$$

where $s = 0.94$ is the proportionally factor.

The solutions of the approximated equation (9) with (10) are given by

$$p_{bsd} = -\frac{1}{2}g_s\sqrt{v_{bs0}^2 + v_{bz0}^2}v_{bs0}T^2 + v_{bs0}T + p_{bs0} \tag{11}$$

$$p_{bzd} = -\frac{1}{2}g_zT^2 + v_{bz0}T + p_{bz0}, \tag{12}$$

where $g_s := \frac{C_D\pi\rho r^2 s}{2m}$ and $T > 0$ is the hitting time. The purpose is to obtain the 4 variables of $\boldsymbol{v}_b' = \boldsymbol{v}_{b0} \in \mathbb{R}^3$ and T by using 3 equations of (11), (12) and (8). In order to eliminate the redundancy, we introduce the relationship of the elevation angle of the ball:

$$v_{bz0} = K_\theta v_{bs0}, \tag{13}$$

where $K_\theta > 0$ is the free parameter. Combining (11), (12) and (13) leads to

$$b_2T^4 + 2b_1T^2 + b_0 = 0, \tag{14}$$

where

$$\begin{aligned}b_2 &:= -g_sg_z^2\sqrt{1 + K_\theta^2}\\ b_1 &:= 2g_z\left(1 + g_zp_{bz0}\sqrt{1 + K_\theta^2}\right)\\ b_0 &:= -4p_{bz0}\left(1 + \frac{b_1}{2g_z}\right) - 8p_{bsd}.\end{aligned} \tag{15}$$

Note that $p_{bzd} = 0$ and $p_{bs0} = 0$. Solving (14) with respect to the hitting time T yields

$$T = \sqrt{\frac{-b_1 + \sqrt{b_1^2 - b_2b_0}}{b_2}}. \tag{16}$$

From T of (16), the velocity just after the rebound of the racket is given by

$$\begin{aligned}v_{bz0} &= \frac{g_zT^2 - 2p_{bz0}}{2T}\\ \begin{bmatrix}v_{bx0}\\ v_{by0}\end{bmatrix} &= v_{bs0}\frac{\boldsymbol{p}_{bd0}}{\|\boldsymbol{p}_{bd0}\|}, v_{bs0} = \frac{1 - \sqrt{1 - 2g_zp_{bsd}\sqrt{1 + K_\theta^2}}}{g_zT\sqrt{1 + K_\theta^2}}\end{aligned} \tag{17}$$

The obtained velocity $\boldsymbol{v}_b' = [v_{bx0}, v_{by0}, v_{bz0}]^{\mathrm{T}}$ is used in the next subsection.

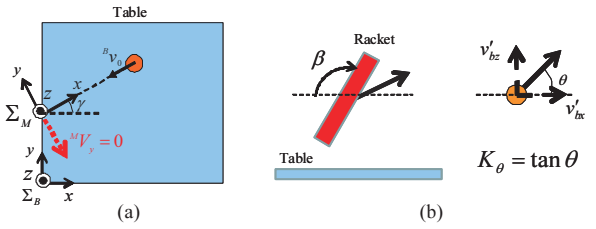

Fig. 10. (a) The virtual constraint for the racket velocity and (b)the free parameters in the motion determination of the racket.

C. Determination of Velocity and Orientation of Racket

Suppose that the velocities just before the rebound, $(\boldsymbol{v}_b, \boldsymbol{\omega}_b)$ and the translational velocity just after the rebound, $\boldsymbol{v}'_b$ are given. Since the rotational velocity $\boldsymbol{\omega}'_b$ is ignored in the previous subsection, it is sufficient to consider the upper equation of (2):

$$\boldsymbol{R}_R^{\mathrm{T}}(\boldsymbol{v}'_b - \boldsymbol{V}_R) = \bar{\boldsymbol{A}}_v \boldsymbol{R}_R^{\mathrm{T}}(\boldsymbol{v}_b - \boldsymbol{V}_R) + \bar{\boldsymbol{B}}_v \boldsymbol{R}_R^{\mathrm{T}} \boldsymbol{\omega}_b \qquad (18)$$

In addition to (18), the following virtual constraint is introduced:

$$-V_{Rx}\sin\gamma + V_{Ry}\cos\gamma = 0,\ \gamma := \tan^{-1}\frac{v_{by}}{v_{bx}} \qquad (19)$$

which is illustrated in (a) of Fig. 10. The frame Σ_M is defined as the x-axis of the frame Σ is rotated about the z-axis through γ. Note that the x-axis of Σ_M is opposite direction of the flying ball in the (x, y) plane. The constraint (19) represents ${}^M V_{Ry} = 0$, i.e., the normal velocity with respect to the ball trajectory in the (x, y) plane equals 0. The left superscript stands for the frame in which the variable is expressed.

The purpose is to obtain the 5 variables of the angle (β, α) and the velocity $\boldsymbol{V}_R \in \mathbb{R}^3$ by using 4 equations of (18) and (19). In order to eliminate the redundancy, we deal with the elevation angle β as the free parameter. Combining (18) and (19) leads to the following quartic equation with respect to the angle of direction α:

$$c_4 \tan\alpha^4 + c_3 \tan\alpha^3 + c_2 \tan\alpha^2 + c_1 \tan\alpha + c_0 = 0, \quad (20)$$

where

$$\begin{aligned}
&c_4 = d_4^2,\ c_3 = 2d_2d_4,\ c_2 = d_2^2 + 2d_1d_4,\\
&c_1 = 2d_1d_2,\ c_0 = d_1^2 - d_3^2\\
&d_1 = ({}^M v'_y - {}^M v_y + a\,{}^M v_y)(1 + e_n)\\
&d_2 = -({}^M v_z - {}^M v'_z + {}^M v_x - {}^M v'_x)(1 + e_n - a)\sin\beta\\
&d_3 = ra\,{}^M\omega_x(1 + e_n)\cos\beta - ra\,{}^M\omega_z(1 + e_n)\sin\beta\\
&d_4 = a(e_r\,{}^M v_y + {}^M v'_y).
\end{aligned}$$

The equation (20) is solved by Ferrari's Solution [16]. By the obtained α and the free parameter β, the racket velocity $\boldsymbol{V}_R$ is easily solved with (19).

D. Minimization of Racket Angle relative to the free parameters

In the inverse problems of the motion determination of the racket, we have the two free parameters (β, K_θ) as in (b) of Fig. 10, which are related to the elevation angles of the racket and the velocity just after the rebound of the racket. The candidates of the racket velocity are calculated within the 330 combinations of $90 \le \beta < 135$ [deg] (the step: 1.5 [deg]) and $30 \le \theta \le 60$ [deg] (the step: 3 [deg]). The time amount of the iteration of the calculation is less than 1 [ms].

VI. Experimental Results

The overview of the experimental system is shown in (a) of Fig. 11. The green square is the target area on the opponent' court, which is the number 9 of the areas divided to 9 areas as in (b) of Fig. 11. The shot balls rebound on the blue area in the court of the robot.

The robot control starts from the time when the desired angle and velocity of the racket are obtained by the motion determination. The desired trajectory from a standby coordinates to the desired ones are interpolated by the 4th order polynomial equation of time. The standby position is $[0.53, 0.39, 0.39]^{\mathrm{T}}$ [m] and the angles are $\beta = 90$ and $\alpha = 0$ [deg]. The initial conditions of the flying ball are $\boldsymbol{p}_b = [2.68, 0.35, 0.35]^T$ [m], $\boldsymbol{v}_b = [-5.92, -0.72, -0.05]^{\mathrm{T}}$ [m/s] and $[377, -3111, 0]^{\mathrm{T}}$ [rpm].

The experiment result is illustrated in Fig. 12. The red square is the racket at the hitting time. The green and blue lines represent the racket trajectories before and after the hitting. The black line is the ball trajectory. The ball trajectory is measured by two CCD cameras (150fps) of a real-time tracking system, Radish(Library, Co.). The positions of the racket and the racket at the hitting are $[-0.048,\ 0.488,\ 0.275]^{\mathrm{T}}$ and $[-0.007,\ 0.446,\ 0.288]^{\mathrm{T}}$ [m]. Since the error between them is about 60 [mm] and the size of the racket is 160×150 [mm], the error is within the racket plane. Furthermore, the result of the position on the table is $[2.027,\ 1.236,\ 0]^{\mathrm{T}}$ and the desired one is $[2.055, 1.271, 0]^{\mathrm{T}}$. The error distance of about 45 [mm] demonstrates the effectiveness of the method.

The time history of the position and angle of the racket is shown in Fig. 13. The red and blue lines represent the desired and real trajectories. The first and second columns are the position and the yaw-pitch-roll parameterization of the angle. The green circles represent the hitting time. There is a little tracking errors and the real values are close to the desired ones at the hitting time. The tracking performance

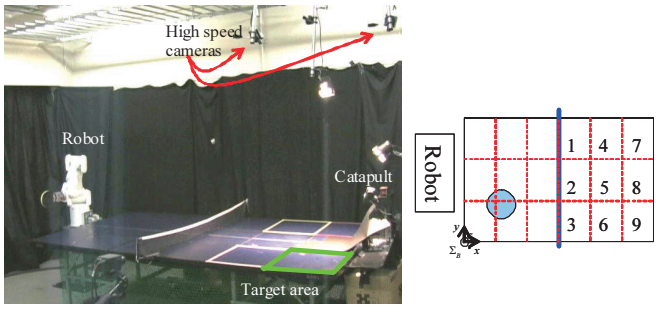

Fig. 11. The experimental system and the target areas.

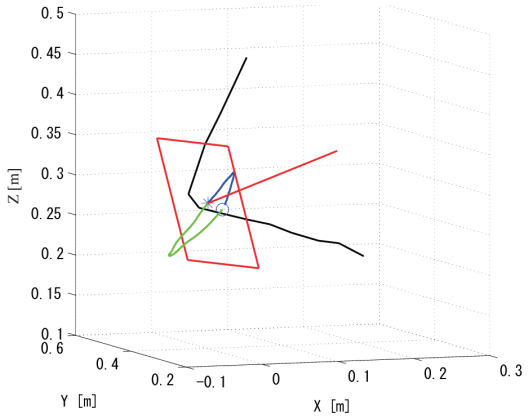

Fig. 12. Hitting the ball in 3D view.

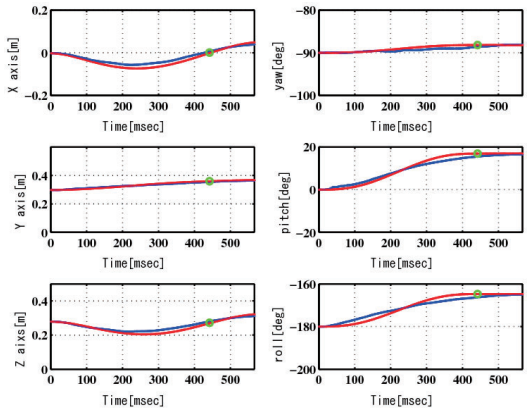

Fig. 13. The trajectories of the position and angle of the racket.

TABLE I

RATE OF SUCCESS

Area	1	2	3	4	5
Rate of success	56%	87%	60%	68%	67%
Area	6	7	8	9	-
Rate of success	25%	46%	50%	60%	-

of the velocity is expressed by the error 0.17 [m/s] of its magnitude at the hitting time. This error may cause the error of the arrival of point of the ball on the table.

The success rates of the hitting the ball to the each area in the opponent's court are shown in Table I. The each number of trial are 15–20 and the averaged success rate is 58%. This rate is bigger than the one of the authors 47%. The continuous hitting can be watched in [17].

VII. CONCLUSIONS

In this paper, we have developed the robotic table tennis system based on the physical models of the ball motion with the our developed real-time measuring method of the flying rotated ball. In order for the robot with a racket to hit the ball to a target point, the determination method of the racket motion has been proposed. The motion determination method has been performed by two sub inverse problems of the physical models. The effectiveness of the proposed method has been verified by the experiments.

Feature work is discussed here. The prediction of the ball trajectory is executed by only the velocities at the time when the ball is shot. Therefore, the measurement error effects on the accuracy very much. Other vision cameras to be able to measure widely is necessary for the improvement. The rotational velocity is not considered in the determination of the racket motion while it is considered in the prediction. Controlling the rotational velocity of the hit ball is necessary for the robot to hit strongly.

REFERENCES

[1] M. Mason and K. Lynch, "Dynamic manipulation," in *Proceedings of IEEE/RSJ International Conference on Intelligent Robots and Systems*, vol. 1, 1993, pp. 152 –159 vol.1.

[2] T. Tamaki, T. Sugino, and M. Yamamoto, "Measuring ball spin by image registration," in *Proc. 10th Frontiers of Computer Vision*, 2004, pp. 269–274.

[3] Z. Zhang, D. Xu, and J. Yu, "Research and latest development of ping-pong robot player," in *7th World Congress on Intelligent Control and Automation*, 2008, pp. 4881 –4886.

[4] F. Miyazaki, M. Takeuchi, M. Matsushima, T. Kusano, and T. Hashimoto, "Realization of the table tennis task based on virtual targets," in *Proceedings of IEEE International Conference on Robotics and Automation*, 2002.

[5] M. Matsushima, T. Hashimoto, M. Takeuchi, and F. Miyazaki, "A learning approach to robotic table tennis," *IEEE Transactions on Robotics*, vol. 21, no. 4, pp. 767 – 771, 2005.

[6] H. Hashimoto, F. Ozaki, K. Asano, and K. Osuka, "Development of a pingpong robot system using 7 degrees of freedom direct drive arm," in *Proc. Int. Conf. on Industrial Electronics, Control and Instrumentation*, 1987, pp. 608–615.

[7] R. L. Anderson, *A robot ping-pong player: experiment in real-time intelligent control*. Cambridge, MA, USA: MIT Press, 1988.

[8] Z. Zhang, D. Xu, and M. Tan, "Visual measurement and prediction of ball trajectory for table tennis robot," *IEEE Transactions on Instrumentation and Measurement*, vol. 59, no. 12, pp. 3195 –3205, 2010.

[9] P. Yang, D. Xu, H. Wang, and Z. Zhang, "Control system design for a 5-dof table tennis robot," in *11th International Conference on ICARCV*, 2010, pp. 1731 –1735.

[10] Y. Nakabo, M. Ishikawa, H. Toyoda, and S. Mizuno, "1ms column parallel vision system and its application of high speed target tracking," in *Proc. IEEE Int. Conf. Robot. Automat.*, 2000, pp. 650–655.

[11] Y. Watanabe, T. Komuro, S. Kagami, and M. Ishikawa, "Multi-target tracking using a vision chip and its applications to real-time visual measurement," *Journal of Robotics and Mechatronics*, vol. 17, no. 2, pp. 121–129, 2005.

[12] A. Nakashima, Y. Tsuda, C. Liu, and Y. Hayakawa, "A real-time measuring method of translational/rotational velocities of a flying ball," in *Proceeding of 5th IFAC Symposium on Mechatronic Systems*, 2010, pp. 732–738.

[13] C. Liu, Y. Hayakawa, and A. Nakashima, "A registration algorithm for on-line measuring the rotational velocity of a table tennis ball," in *Proceeding of IEEE/RSJ International Conference on Intelligent Robots and Systems*, 2011, to be submitted.

[14] J. Nonomura, A. Nakashima, and Y. Hayakawa, "Analysis of effects of rebounds and aerodynamics for trajectory of table tennis ball," in *Proceedings of SICE Annual Conference*, 2010, pp. 1567 –1572.

[15] A. Nakashima, Y. Ogawa, Y. Kobayashi, and Y. Hayakawa, "Modeling of rebound phenomenon of a rigid ball with friction and elastic effects," in *Proc. IEEE Amer. Cont. Conf.*, 2010, pp. 1410–1415.

[16] S. MacLane and G. Birkoff, *ALGEBRA*. London: Collier Macmillan, 1967.

[17] A. Nakashima. (2011) Mpeg video for iros2011. [Online]. Available: http://www.haya.nuem.nagoya-u.ac.jp/˜akira/iros2011.mp4